JOURNAL OF Materials CHEMISTRY

Composite materials obtained by ion irradiation: Mn implantation in silica glass

Simona Barison,[a] Giancarlo Battaglin,[b] Renzo Bertoncello,[a] Elti Cattaruzza,*[b] Anna Mascolo,[c] Paolo Mazzoldi,[c] Marco Ruzzi[d] and Fiorella Trivillin[a]

[a]*Unità I.N.S.T.M., Dipartimento di Chimica Inorganica, Metallorganica ed Analitica, via Loredan 4, 35131 Padova, Italy*
[b]*Unità I.N.F.M., Dipartimento di Chimica Fisica, Dorsoduro 2137, 30123 Venezia, Italy. E-mail: cattaruz@unive.it*
[c]*Unità I.N.F.M., Dipartimento di Fisica, Università di Padova, via Marzolo 8, 35131 Padova, Italy*
[d]*Dipartimento di Chimica Fisica, Università di Padova, via Loredan 2, 35131 Padova, Italy*

Received 13th July 1999, Accepted 10th September 1999

Ion implantation in silica is a useful way to generate unusual properties in glasses. To use ion implantation as a synthesis technique, it is necessary to understand the dynamics of the process. Silica glass samples, implanted with Mn at 38 keV energy and fluences of 1×10^{16}, 5×10^{16} and 10×10^{16} ions cm^{-2} were investigated mainly by X-ray photoelectron (XPS), X-ray-excited Auger electron (XE-AES) and UV-photoelectron (UPS) spectroscopies. Rutherford backscattering (RBS) and secondary ion mass spectrometry (SIMS) measurements, optical absorption and electron paramagnetic resonance (EPR) investigations were also performed. Mn silicate is present in all samples, while in the 5×10^{16} and 10×10^{16} samples Mn silicide compounds form in the most damaged region. These findings give further support to the *two-step* model as a simple method to predict the final compounds resulting from ion irradiation of a solid matrix.

1 Introduction

The implantation of metal ions on a solid target is an effective way to confer unusual magnetic, optical and/or catalytic properties to materials. Metal–ion implantation can modify the physical–chemical properties of a thin layer of the matrix, forming metallic nanoparticles and/or by a reaction with the surrounding matrix atoms, forming compounds. Study of the ion–matrix interaction is a fundamental key to understanding the ion implantation process with the aim of synthesizing new materials: under the same implantation conditions, different elements react with the same matrix in different ways. In glass substrates, as observed for Cr, Ni and Pd implantations,[1–4] the final compounds observed depend also on the implantation fluence, *i.e.*, on the dopant concentration in the host matrix.

As a useful description of the ion irradiation process we consider the so-called *two-step* model.[3,5] The implantation process is proposed to be separated into two independent steps: a high-energy (physical) step, characterized by ballistic effects, and a low-energy (chemical) step, in which chemical driving forces are predominant. In this way, the final configuration is predictable using a thermodynamic approach. The *two-step* model can be a useful theoretical tool to predict the final physical–chemical modification of the implanted material.

Investigations of Mn-implanted silica samples through EPR, IR and UV–VIS spectroscopies have already appeared in the literature:[6–8] the formation of both Mn metallic nanoparticles and Mn oxide compounds was assumed but not verified by chemical analyses. Here, we investigate in detail the chemical interaction between implanted Mn atoms and silica substrates, mainly by using photoelectron spectroscopy techniques.

2 Experimental

Type III (Tetrasil A) silica slides were implanted at room temperature with Mn ions of 38 keV energy and fluences of 1×10^{16}, 5×10^{16} or 10×10^{16} ions cm^{-2}. The current density was maintained at <2 μA cm^{-2}. During irradiation, the sample temperature increase did not exceed *ca.* 30 °C. Ion implantations were performed at the Centre de Spectrométrie Nucléaire et Spectrométrie de Masse (Orsay, France). The mean projected range, R_p, and the range straggling, ΔR_p, calculated by the TRIM code[9] are 36 and 12 nm, respectively.

Samples were investigated by X-ray photoelectron, X-ray-excited Auger electron and UV photoelectron spectroscopies (XPS, XE-AES and UPS, respectively), optical absorption investigation, EPR, Rutherford backscattering (RBS) and secondary ion mass (SIMS) spectrometries.

XPS and XE-AES measurements were obtained on a VG Escalab Mk II spectrometer using non-monochromated Al-K$\alpha_{1,2}$ radiation (1486.6 eV). Some XPS measurements were performed using monochromated Al-K$\alpha_{1,2}$ radiation, by using a Perkin-Elmer Φ 5600ci spectrometer. The working pressure was $<1\times10^{-7}$ Pa. Depth profiles of the different elements were carried out by cycles of Ar^+ sputtering at an energy of 3 keV. The sputtering rate was estimated to be *ca.* 0.2 nm min^{-1}. No evidence of preferential sputtering was revealed. For charging effects, the binding energy (E_b) of the O 1s peak of silica (532.7 eV) was used as an internal reference. During the depth profile, detailed scans were obtained for the C 1s, O 1s, Si 2p, Si KLL, Mn 2p, Mn 3s, Mn 3p and Mn LMV regions. The spectra were analysed with a Shirley-type background subtraction[10] and were fitted using a program adopting Gaussian–Lorentzian peak shapes. Samples of manganese silicide as obtained after annealing (*ca.* 800 °C for 3 h) of an evaporated Mn layer (*ca.* 80 nm thick) on a polycrystalline silicon substrate were used as reference standards for XPS and XE–AES peaks.[11] Annealing was performed in a vacuum furnace. Standards of silicon and fused silica were also used.

The VG Escalab Mk II spectrometer is also equipped with an ultraviolet He lamp (He II: 40.81 eV radiation energy) for the

UPS investigation of the valence band. Because of the insulating characteristic of our samples, during UPS analyses it was necessary to reduce the charging effect with a low-energy electron gun. This caused modifications of the bands, leading to the impossibility of comparison of the absolute position and intensity of the spectra. We could thus compare only the shapes of different spectra.

Optical absorption spectra were recorded in the 200–800 nm wavelength range with a Varian CARY 5E UV–VIS–NIR dual-beam spectrophotometer.

EPR spectra were recorded with a Bruker ER 200D EPR X-band spectrometer equipped with a standard TE_{102} rectangular cavity and nitrogen flow cryostat.

RBS analyses were performed at Laboratori Nazionali INFN of Legnaro (Italy) using a 2.2 MeV $^4He^+$ beam. Spectra were taken at a backscattering angle of 160° and with an angle of 55° between the sample normal and the beam direction, in order to enhance the depth profile scale.

SIMS analyses were performed with two different spectrometers. SIMS I measurements were recorded with a CAMECA ims-4f ion microscope equipped with a normal incidence electron gun for charge compensation. Concentration depth profiles were obtained by 14.5 keV Cs^+ bombardment and by negative-ion detection. SIMS II measurements were performed at the CNR-IPELP Institute of Padova (Italy); the depth profiles were obtained by 6 keV O^+ bombardment.

3 Results and discussion

In all the composites the Mn-retained fluence is comparable with the nominal implantation fluence, as indicated by RBS measurements.

3.1 1×10^{16} Mn^+ cm^{-2} irradiated silica sample

The XPS depth profile of Mn atoms (Fig. 1) shows an approximately Gaussian shape with a maximum atomic concentration of *ca.* 5%. The Mn irradiation does not modify either the silica stoichiometry or the chemical state of the silica substrate: throughout the depth profile, the O/Si atomic ratio and the Si α parameter [$\alpha = E_b$ of Si 2p + kinetic energy (KE) of Si KLL] are in agreement with unimplanted silica values.[3,12,13] The O 1s band shape indicates the presence of only one chemical species for oxygen atoms, *i.e.*, SiO_2. Other species, if present, involve a low amount of oxygen atoms (< *ca.* 10% with respect to that of SiO_2).

The oxidation state of Mn atoms was determined by examining the Mn 2p E_b values and the Mn α parameter ($\alpha = E_b$ Mn $2p_{3/2}$ + KE Mn LMV). Along the whole profile, the E_b of Mn $2p_{3/2}$ and Mn $2p_{1/2}$ peaks are 643.0 ± 0.2 and 655 ± 0.2 eV, respectively. The Mn α parameter is 1224.0 ± 0.3 eV. By comparison with literature data[13–15] and a Mn silicate standard, the detected values suggest the presence of Mn silicate: the Mn implanted atoms react with the silica substrate. No other Mn compounds are present: in particular, no formation of metallic particles is detected. The XPS and UPS investigations of the valence band confirm the absence of metallic Mn: the spectra do not reveal significant differences when compared to the unimplanted silica valence band structure. The Mn 3s and 3p spectra, recorded by using a monochromated Al X-ray source, reveal a multiplet splitting effect: the Mn 3s signal is split with a separation of 6.3 eV. Such a separation indicates a 2+ oxidation state for Mn and an ionic character of the Mn–O bond.[16]

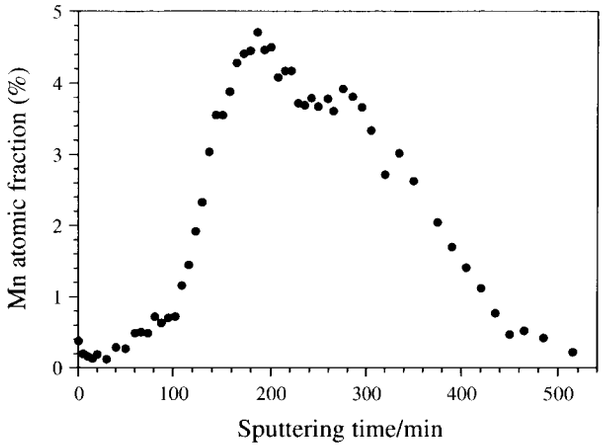

Fig. 1 In-depth profile of the Mn atomic fraction for the 1×10^{16} ions cm^{-2} Mn-implanted silica sample.

These findings are supported by results of the other investigation techniques. RBS and SIMS investigations indicate a Mn concentration depth profile very similar to that obtained by XPS. Positive ion SIMS II spectra, qualitatively similar for all the implanted samples, exhibit signals related to $MnSiO_x^+$ ($1 \leqslant x \leqslant 3$) ion clusters. This is in agreement with the formation of Mn silicates in the solid matrix (as observed by XPS, XE-AES and UPS analyses) because such ion clusters have a very low probability of forming after sputtering. We conclude that at this implantation fluence the silica substrate is largely unmodified: Mn atoms probably react at slightly damaged regions, forming silicate species. However, the absence of an O 1s component typical of silicate species in the XPS spectra, is reasonably attributable to the low concentration of Mn.

3.2 5×10^{16} Mn^+ cm^{-2} irradiated silica sample

The XPS Mn depth profile [Fig. 2(a)] shows a maximum atomic fraction of *ca.* 18%: this maximum concentration region corresponds to the region of maximum damage of the substrate, as confirmed by TRIM. In this sample the ion irradiation induces a modification of the stoichiometry and

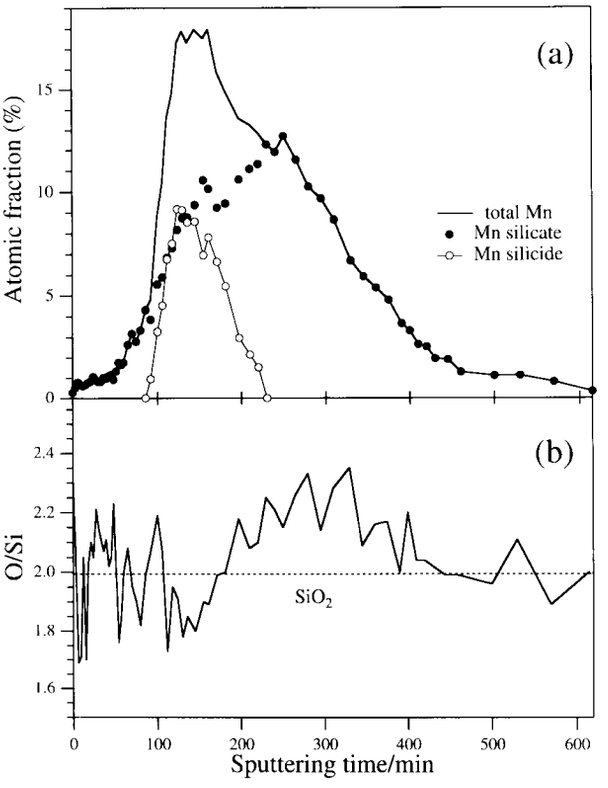

Fig. 2 (a) In-depth profile of Mn atomic fraction for the 5×10^{16} ions cm^{-2} Mn-implanted silica sample with separation of silicide and silicate species and (b) in-depth profile of O/Si ratio.

chemical state of the silica substrate. The most evident effect is the displacement of atoms of the lighter element constituting the substrate (oxygen) towards greater depths inside the sample. Such behaviour has been already observed for chromium and titanium implantation in silica.[3,17] The O/Si ratio [Fig. 2(b)] is <2 in the highly-damaged zone and increases at greater depths, reaching values around 2.3. Moreover, the mean value of the O/Si ratio in the whole implanted region is >2. This indicates a penetration of oxygen atoms inside the heavily damaged matrix, because of exposure to the atmosphere after implantation.[18] The Si α parameter values vary with the depth: in the region of high Mn concentration the Si α parameter shows values *ca.* 0.6 eV higher than characteristic for unimplanted silica (SiO_2: 1711.8 ± 0.3 eV). This behaviour is due to a lowering of the oxidation state of Si.[19]

The oxygen and silicon XPS bands reveal the formation of other compounds in addition to silica. At depths where the Mn atomic fraction is $>10\%$, the O 1s peak shows a shoulder at lower E_b, owing to the presence of a component centred at 531.0 ± 0.2 eV. This is related to the chemical interaction between Mn and O atoms forming Mn silicate, not oxide: in fact, for Mn oxide the O 1s band is centred at values lower than 530 eV.[13] Moreover, in the oxygen-poor region, in addition to the component related to SiO_2, the Si 2p spectrum has a clearly visible second component at $E_b = 98.9 \pm 0.2$ eV (Fig. 3), and the Si KLL band also shows a second component [Fig. 4(a)]. The corresponding Si α parameter is 1716.6 ± 0.3 eV, *i.e.*, different from that of SiO_2 or metallic Si (1715.6 ± 0.2 eV from a silicon standard), as already observed.[3,5,17] The same value was also observed in the Mn silicide standard. Therefore these second components of the Si peaks can be attributed to silicide formation. In the Mn 2p spectra [Fig. 4(b)] a second component appears at the same depths. After the fitting procedure, two different doublets were distinguished in the Mn 2p spectrum. The first has a Mn $2p_{3/2}$ component centred at $E_b = 643.0 \pm 0.2$, the same value as found in the 1×10^{16} sample, thus indicating the presence of a Mn silicate. The E_b of the Mn $2p_{3/2}$ peak of the second doublet is *ca.* 638.6 eV. By comparing this value with both literature data[13–15] and our standards and by observing that at these depths the Mn LMV band broadens and shifts towards values characteristic of silicide species, it is deduced that the second component of the Mn $2p_{3/2}$ signal is mainly due to the formation of Mn silicide. From a quantitative analysis of the lower E_b of Mn and Si components, the average silicide composition is Mn_3Si.

XPS analyses indicate that no metallic Si is present in the sample. However, it is not possible to completely exclude the presence of metallic Mn because of the very similar position of Mn $2p_{3/2}$ and LMV bands for metallic and silicide species.[13] As already described, the detection of SIMS II signals related to $MnSiO_x^+$ ($1 \leqslant x \leqslant 3$) ion clusters is in accord with the formation of Mn silicates inside the matrix. However, it is not possible to obtain by SIMS II any evidence of the presence of silicide compounds, since sputtering effects are unpredictable for these species. UPS analyses reveal small modifications in the valence band of this sample when compared to unimplanted silica.[20] Particularly, changes in the structure of non-bonding O 2p signals between 7 and 14 eV are observed. These variations can be attributed to the presence of the Mn silicate species and/or to a modification of the silica structure by ion irradiation. The appearance of a small component close to 0 eV can be ascribed to the Mn 3d band of silicide species.[21]

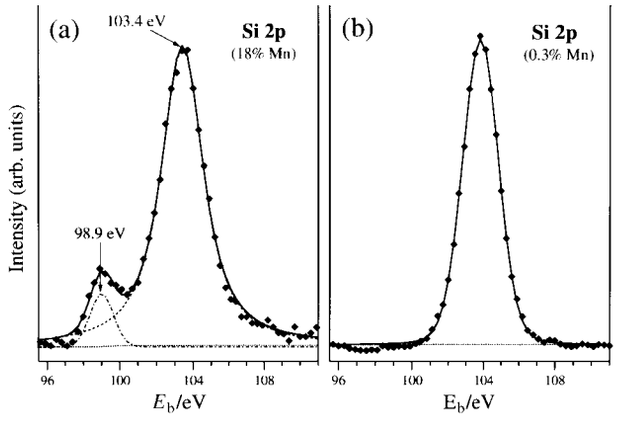

Fig. 3 (a) XPS Si 2p signal recorded for the 5×10^{16} ions cm^{-2} Mn-implanted silica sample at the depth where the Mn concentration is maximum and (b) Si 2p signal recorded at the end of the Mn depth profile.

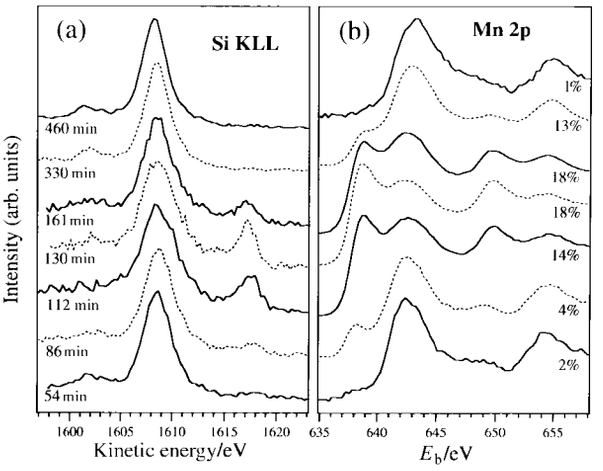

Fig. 4 (a) Si KLL signals recorded at different depths for the 5×10^{16} ions cm^{-2} Mn-implanted silica sample (sputtering time is indicated) and (b) Mn 2p signals recorded at the same depths (corresponding Mn atom% is indicated).

3.3 10×10^{16} Mn^+ cm^{-2} irradiated silica sample

The chemical and physical investigations performed on samples implanted with a fluence of 10×10^{16} suggest a situation very similar to the 5×10^{16} cm^{-2} irradiation. The very high fluence irradiation produces a remarkable surface

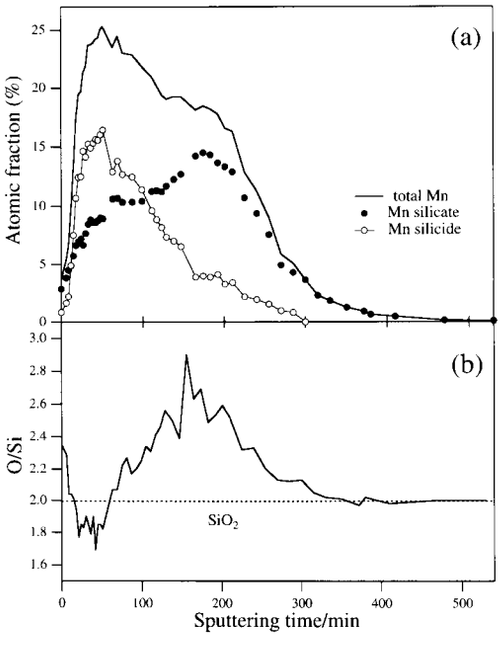

Fig. 5 (a) In-depth profile of Mn atomic fraction for the 10×10^{16} ions cm^{-2} Mn-implanted silica sample, with separation of silicide and silicate species and (b) in-depth profile of O/Si ratio.

erosion by ion sputtering, clearly evident in the XPS depth profile shown in Fig. 5(a). Moreover, now there are more marked variations of the O/Si ratio than in the previous sample [Fig. 5(b)]. XPS and XE-AES measurements show the presence of compounds already observed in the 5×10^{16} sample, with a higher relative concentration of the silicide species. Silicides are already present at the sample surface. The silicide species has the same mean stoichiometry as previously (Mn_3Si).

The presence of silicide species is related to the oxygen deficiency and to the high Mn concentration. The oxygen deficiency can be attributed to irradiation-induced damage, as suggested by the damage depth profile evaluation obtained by TRIM code (Fig. 6).

The UPS valence bands show substantial differences when compared to that of the unimplanted silica (Fig. 7) and of the 5×10^{16} sample. In the first part of the implanted region [Fig. 7(a)], where the silicide compounds have a high concentration, the valence band is very different from that of unimplanted silica and its shape resembles that of Mn silicide.[21] UPS valence bands of silica containing metallic nanoparticles exhibit characteristic features at the Fermi edge, in particular a marked rise of the photoelectron signal around 0 eV, as observed in Ni-[22] and Pd-implanted silica samples:[4] the spectra shown in Fig. 7 do not exhibit this peculiarity. At depths where the concentration of Mn is still high but the silicide compounds have a low concentration [Fig. 7(b)], the valence band shape is closer to that of silica.

We propose that the lack of metallic species is due to the high reactivity of Mn with the silica substrate. For Mn ion implantation in silica, Hosono[23] predicts the formation of Mn metallic colloids. In terms of implantation defects, Hosono[24] predicted the formation of Si–Si bonds to be the predominant defect induced by Mn irradiation of silica. These predictions are, however, in disagreement with our experimental evidence. Using the *two-step* model we predict the chemical products of the implantation process simply from the chemical reactivity of Mn. Since the temperature of our samples during irradiation was only slightly higher than room temperature, we assume a temperature $T=298$ K for our considerations. If we calculate, starting from tabulated Gibbs free energy (ΔG_T^0) values,[25] the actual value for chemical reactions involving Mn and the silica substrate, we observe that among all the thermodynamically allowed processes, the most favoured lead to the formation of Mn silicides and $MnSiO_3$. Some allowed chemical reactions are listed below.

$$2Mn+SiO_2\rightarrow Mn+Si+MnO_2 \qquad \Delta G_{298\,K}{}^0=-93\ \text{kJ mol}^{-1}$$

$$2Mn+SiO_2\rightarrow MnSi+MnO_2 \qquad \Delta G_{298\,K}{}^0=-157\ \text{kJ mol}^{-1}$$

$$2Mn+3SiO_2\rightarrow Si+2MnSiO_3 \qquad \Delta G_{298\,K}{}^0=-397\ \text{kJ mol}^{-1}$$

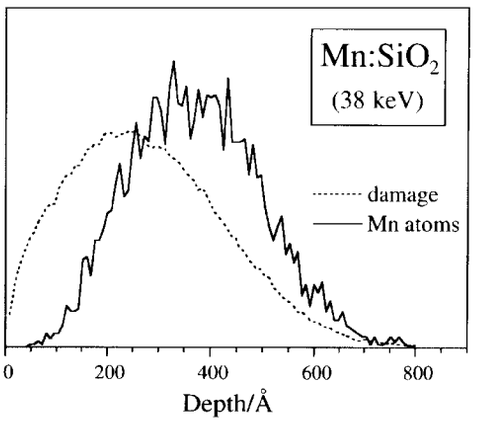

Fig. 6 Irradiation damage and Mn atom depth profiles as calculated by the TRIM code.

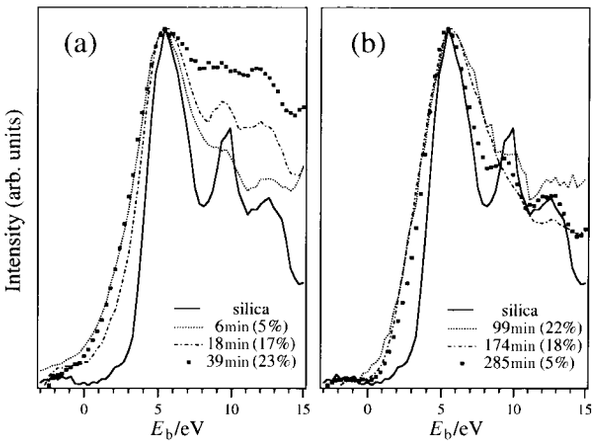

Fig. 7 (a) UPS valence bands for the 10×10^{16} ions cm^{-2} Mn-implanted silica sample recorded at different depths: from the surface to the depth for which the Mn atomic percentage is maximum and (b) beyond the depth for which the Mn atomic percentage is maximum. Sputtering times and corresponding Mn atomic fractions are reported.

$$3Mn+3SiO_2\rightarrow Mn+Si+2MnSiO_3 \qquad \Delta G_{298\,K}{}^0=-638\ \text{kJ mol}^{-1}$$

$$3Mn+SiO_2\rightarrow MnSi+2MnO \qquad \Delta G_{298\,K}{}^0=-651\ \text{kJ mol}^{-1}$$

$$3Mn+3SiO_2\rightarrow MnSi+2MnSiO_3 \qquad \Delta G_{298\,K}{}^0=-702\ \text{kJ mol}^{-1}$$

$$5Mn+3SiO_2\rightarrow Mn_3Si+2MnSiO_3 \qquad \Delta G_{298\,K}{}^0=-1228\ \text{kJ mol}^{-1}$$

The prediction of the *two-step* model is in very good agreement with what is experimentally observed: moreover, chemical kinetic aspects do not appear to play an important role in determining the final compounds obtained. However, in such a prediction of the products of ion implantation simply from calculations of the $\Delta G_T{}^0$ values of the possible reactions, the damage effects induced by ion irradiation in the matrix have been neglected. To determine more fully the chemical reactions that genuinely describe the ion implantation process, we must analyse the chemical species and the stoichiometric coefficients as obtained by quantitative XPS analysis. Obviously, different depths of the sample are characterized by different species and different quantitative coefficients. At the depth of the maximum Mn concentration, we estimate the following approximate reaction:

$$25Mn+27SiO_{1.8}\rightarrow 5.5Mn_3Si+8.5MnSiO_3+13SiO_{1.7}$$

At the depth of the maximum Mn silicate concentration, where the O/Si ratio reaches its maximum value, we estimate:

$$19Mn+8.5O+14.8SiO_2\rightarrow 2.1Mn_3Si+12.7MnSiO_3$$

Here, the accumulation of oxygen atoms in a low-damaged region (Fig. 6) should be *via* peroxide radicals,[26] rather than a real modification of the silica stoichiometry. A correct evaluation of $\Delta G_{298\,K}{}^0$ for these reactions is however very complicated to obtain, mainly because of the difficulty in estimating the Gibbs energy data for non-stoichiometric species.

To evaluate the paramagnetic properties of this sample, an X-band EPR spectrum was recorded at two different temperatures. At 260 K (Fig. 8) the spectrum consists of a broad Lorentzian line centred at 340 mT ($g=2.000$) with a peak-to-peak linewidth of 15.6 mT. The spectrum recorded at 145 K does not show a significant difference, except for a slightly higher linewidth (16.9 mT). These spectra are very similar to those observed for a 160 keV Mn-implanted silica[7] and indicate Mn^{2+} ions interacting by spin–spin interactions, similarly to Mn implantation in CdTe.[27] Signals due to E′ defects, *i.e.* oxygen vacancies, and to peroxide radicals[28] were too weak to be detected in our samples. No resolved hyperfine

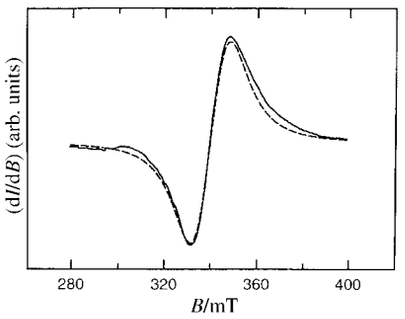

Fig. 8 Experimental (—) and simulated (---) EPR spectra of the 10×10^{16} ions cm^{-2} Mn-implanted silica sample. Temperature: 260 K; microwave resonant field $B_1 = 0.45$ μT.

structure is evident which indicates that Mn^{2+} ions are not isolated or that their concentration is too small to detect. Therefore, the presence of Mn silicide nanoparticles appears likely, similarly to the behavior of Cr- and Ti-implanted silica.[3,5,17] The magnetic properties are characteristic of a *spin-glass*.

4 Conclusions

Ion implantation of manganese in silica glass leads to the formation of a variety of compounds. High implantation fluences give rise to a considerable in-depth diffusion of oxygen atoms. As a consequence, different Mn compounds are formed in the samples at different depths. In the sample irradiated with 1×10^{16} Mn^+ ions cm^{-2}, the in-depth deviation of the O/Si ratio from the stoichiometric value of silica is almost negligible: Mn implanted atoms react with silica to form manganese silicate, $MnSiO_3$. It is likely that they form bridging links between two oxygen atoms. In the samples irradiated with 5×10^{16} and 10×10^{16} Mn^+ ions cm^{-2}, the oxygen diffusion is more marked. At depths where the O/Si ratio is low, the manganese reacts also with silicon to give manganese silicide, in addition to the silicate. The depth profile of Mn atoms does not have a Gaussian shape and accumulation of manganese takes place in the most-damaged region. In all the three samples, there is no evidence for the presence of metallic manganese. In the 10×10^{16} sample, EPR measurements suggest the presence of nanoclusters of Mn silicide.

Ion implantation can be used as a thin film synthesis technique. Possible applications of composite materials obtained by metal ion implantation in silica are, for example, in non-linear and magneto-optical devices. Thus, it is important to formulate theoretical models which are able to describe in a simple way the ion irradiation process. Among them, the *two-step* model is the only one able to predict the formation of silicide species as a consequence of Mn implantation in silica. Moreover, it also predicts the formation of manganese silicate. In conclusion, this thermodynamic approach supplies satisfactory predictions concerning chemical modifications of the solid target: nevertheless, we are well aware that ion irradiation is a process that does not occur under thermodynamic equilibrium conditions.

Work is in progress to test the correctness of the *two-step* model for different ions implanted in silica and, more generally, for different ion–substrate pairs.

Acknowledgements

We are grateful to Dr F. Caccavale (Unità I.N.F.M. di Padova, Dipartimento di Fisica–Università di Padova) for SIMS I measurements, and to Dr M. Fabrizio (I.P.E.L.P.—C.N.R. Padova) for SIMS II measurements and for helpful discussions.

References

1 E. Cattaruzza, F. Gonella, G. Mattei, P. Mazzoldi, G. Battaglin, D. Gatteschi, C. Sangregorio, R. Bertoncello and F. Trivillin, *Proceedings of the XVIII International Conference on Glass*, *San Francisco, CA*, 1998, ed. M. K. Choudhary, N. T. Huff and C. H. Drummond III, Am. Ceram. Soc., Westerville, OH, 1998, **C11,** 13.
2 G. Battaglin, R. Bertoncello, M. Casarin, E. Cattaruzza, P. Colombo, R. Ganzerla, F. Garrido, M. Lenarda, G. Mattei, P. Mazzoldi, F. Trivillin and M. Urbani, *Proceedings of the XVIII International Conference on Glass*, *San Francisco, CA*, *1998*, ed. M. K. Choudhary, N. T. Huff and C. H. Drummond III, Am. Ceram. Soc., Westerville, OH, 1998, **C4,** 117.
3 E. Cattaruzza, R. Bertoncello, F. Trivillin, P. Mazzoldi, G. Battaglin, L. Mirenghi and P. Rotolo, *J. Mater. Res.*, 1996, **11**, 229.
4 G. Battaglin, R. Bertoncello, M. Casarin, E. Cattaruzza, G. Mattei, P. Mazzoldi, F. Trivillin and M. Urbani, *J. Non-Cryst. Solids*, 1999, **253**, 251.
5 R. Bertoncello, A. Glisenti, G. Granozzi, G. Battaglin, F. Caccavale, E. Cattaruzza and P. Mazzoldi, *J. Non-Cryst. Solids*, 1993, **162**, 205.
6 R. F. Haglund, H. C. Mogul, R. A. Weeks and R. A. Zuhr, *J. Non-Cryst. Solids*, 1991, **130**, 326.
7 H. Hosono, R. A. Weeks, H. Imagawa and R. A. Zuhr, *J. Non-Cryst. Solids*, 1990, **120**, 250.
8 R. H. Magruder, S. H. Morgan, R. A. Weeks and R. A. Zuhr, *J. Non-Cryst. Solids*, 1990, **120**, 241.
9 J. P. Biersack and W. G. Eckstein, *Appl. Phys.*, 1984, **34**, 73.
10 D. A. Shirley, *Phys. Rev.*, 1972, **55**, 4709.
11 G. Ottaviani, *Thin Solid Films*, 1986, **140**, 3.
12 *X-Ray Photoelectron Spectroscopy Database*, Version 1.0, National Institute of Standards and Technology, Gaithersburg, MD, 1989.
13 J. F. Moulder, W. F. Stickle, P. E. Sobol and K. D. Bomben, in *Handbook of X-Ray Photoelectron Spectroscopy*, ed. J. Chastain, Perkin Elmer Corp., Eden Prairie, MN, 1992.
14 M. Oku, K. Hirokawa and S. Ikeda, *J. Electron. Spectrosc. Relat. Phenom.*, 1975, **7**, 465.
15 B. R. Strohmeier and D. M. Hercules, *J. Phys. Chem.*, 1984, **88**, 4922.
16 C. S. Fadley and D. A. Shirley, *Phys. Rev. A*, 1970, **2**, 1109.
17 E. Cattaruzza, G. Mattei, P. Mazzoldi, R. Bertoncello, G. Battaglin and L. Mirenghi, *Appl. Phys. Lett.*, 1995, **67**, 2884.
18 G. W. Arnold, G. De Marchi, P. Mazzoldi and G. Battaglin, *Nucl. Instrum. Methods B*, 1996, **116**, 364.
19 T. Hattori, *J. Vac. Sci. Technol. B*, 1993, **11**, 1528.
20 T. H. DiStefano and D. E. Eastman, *Phys. Rev. Lett.*, 1971, **27**, 1560.
21 A. Kakizaki, H. Sugawara, I. Nagakura, Y. Ishikawa, T. Komatsubara and T. Ishii, *J. Phys. Soc. Jpn.* 1982, **51**, 2597.
22 G. Battaglin, R. Bertoncello, E. Cattaruzza, P. Mazzoldi and M. Ricci, unpublished work.
23 H. Hosono, *Jpn. J. Appl. Phys.*, 1993, **32**, 3892.
24 H. Hosono, *J. Non-Cryst. Solids*, 1995, **187**, 457.
25 O. Knacke, O. Kubaschewski and K. Hesselmann, *Thermochemical Properties of Inorganic Substances*, Springer-Verlag, Berlin, Heidelberg, 2nd edn., 1991.
26 H. Hosono and H. Imagawa, *Nucl. Instrum. Methods B*, 1994, **91**, 510.
27 L. Pasimeni, G. Leo and L. Vasanelli, *Solid State Commun.*, 1993, **88**, 317.
28 G. Whichard and R. A. Weeks, *J. Non-Cryst. Solids*, 1989, **112**, 1.

Paper 9/05679C